Click Here for Full Article

Sensitivity of sulfate direct climate forcing to the hysteresis of particle phase transitions

Jun Wang,[1,2] Daniel J. Jacob,[1] and Scot T. Martin[1]

[1]   The effects of solid-aqueous phase transitions on sulfate direct climate forcing (SDCF) are investigated by using both a column model and a global chemical transport model. Aqueous particles have a larger mass extinction efficiency but a smaller backscattered fraction than their solid counterparts. The column model shows that the hysteresis of the phase transition can result in an uncertainty in the SDCF of 20%. The global chemical transport model explicitly accounts for the relative humidity processing of particles and the associated hysteresis. The model also treats the extent of sulfate neutralization by ammonia. For the anthropogenic sulfate, the base case simulation finds that solid particles contribute 41% of the global burden, 26% of the clear-sky optical thickness, 31% of the clear-sky SDCF, and 37% of the full-sky SDCF, a trend that reflects the correlation of solid particles with clear skies. A perturbation to the model, omitting hysteresis by assuming that all particles are aqueous, results in an overestimate of the SDCF by +8% compared to the base case. A converse assumption that crystallization occurs at the deliquescence relative humidity underestimates the SDCF by −8%. A case that assumes that aqueous particles occur whenever the ambient relative humidity exceeds the crystallization relative humidity biases the SDCF by +5%. A case that includes hysteresis but omits the difference in the fraction of radiation backscattered to space by aqueous compared to solid particles changes the SDCF by +15%. Seasonal and regional differences can be much larger. We recommend that the ratio of the sulfate aerosol optical thickness calculated with versus without consideration of particle hygroscopicity be reported as a standard output of SDCF models to facilitate meaningful intercomparisons among different models.

1.   Introduction

[2]   Atmospheric sulfate particles, the largest anthropogenic component of fine particulate matter, reflect solar radiation back to space, thereby cooling the climate [*Charlson et al.*, 1992; *Intergovernmental Panel in Climate Change* (*IPCC*), 2007]. The change caused by sulfate scattering to the upwelling solar irradiance at the top of the atmosphere is referred to as the sulfate direct radiative effect (SDRE) [*Anderson et al.*, 2005]. The anthropogenic component is the sulfate direct climate forcing (SDCF). Literature estimates of the global annual SDCF range from −0.16 to −0.96 W m^{-2} [*IPCC*, 2007]. Reducing the uncertainty of the SDCF is crucial for quantifying the extent to which aerosols can counteract or delay warming by greenhouse gases [*Jacob et al.*, 2005; *Hansen et al.*, 2005; *Crutzen*, 2006].

[3]   In this study, we analyze the effect of the hysteresis of solid-aqueous particle phase transitions on the SDCF, focusing on the sulfate-ammonium system. The phase transition affects the hygroscopic behavior and subsequently the size, the refractive index, and the radiative properties of a particle. An accurate description of phase transitions in ambient air, however, is a challenging task because knowledge of both the relative humidity history and the particle chemical composition is necessary [*Martin*, 2000]. The composition of sulfate-ammonium particles is characterized by the extent of neutralization, defined as $X = [NH_4^+]/2[SO_4^{2-}]$, where the concentrations are in molar units. Sulfuric acid particles ($X = 0$) are aqueous at all relative humidity (RH) values, and they grow by water uptake for increasing RH. In contrast, ammonium-containing particles can be solids at low RH. Crystalline forms include $(NH_4)_2SO_4$ (ammonium sulfate, AS), NH_4HSO_4 (ammonium bisulfate, AHS), and $(NH_4)_3H(SO_4)_2$ (letovicite, LET). As an example of the hysteresis, an AS particle ($X = 1$) exposed to increasing RH becomes aqueous at its deliquescence relative humidity (DRH) of 80% and subsequently grows at higher RH by condensation of water vapor, but if this aqueous particle of $X = 1$ is then

---

[1]School of Engineering and Applied Sciences, Harvard University, Cambridge, Massachusetts, USA.
[2]Now at Department of Geosciences, University of Nebraska–Lincoln, Lincoln, Nebraska, USA.
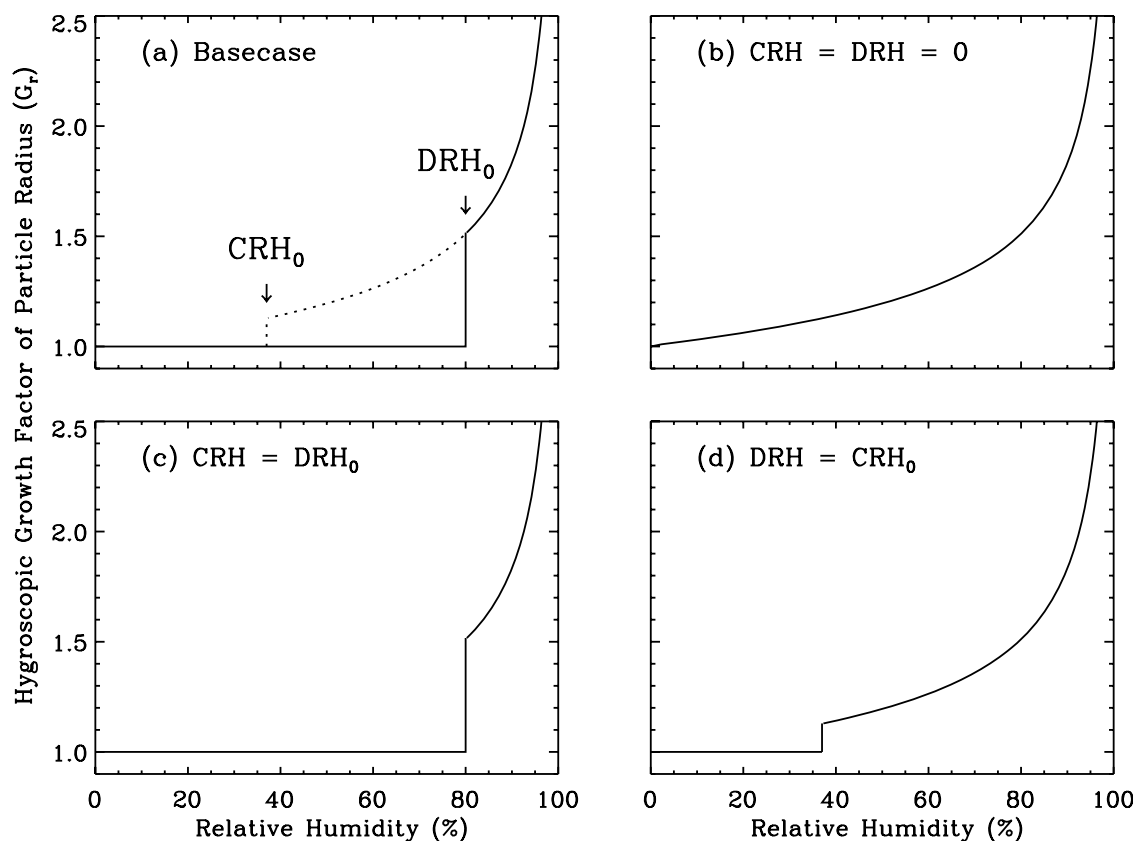
Figure 1. Ammonium sulfate hygroscopic growth factor for increasing RH for (a) a base case and (b–d) three sensitivity analyses. The base case has full consideration of the hysteresis loop between the crystallization relative humidity (CRH_0) and the deliquescence relative humidity (DRH_0), where subscript "0" indicates a reference value of CRH or DRH as measured in the laboratory experiments. For the sensitivity analyses, Figure 1b shows CRH = DRH = 0, Figure 1c shows CRH = DRH_0, and Figure 1d shows DRH = CRH_0. The dotted line in the base case shows the upper side of the hysteresis loop.

exposed to decreasing RH, it gradually shrinks but does not become solid until its crystallization relative humidity (CRH) of 35%. A hysteresis effect thereby arises: solid AS particles at low RH follow the lower side of the hysteresis loop for increasing RH and remain of fixed diameter and solid until ambient RH exceeds the DRH, whereas aqueous particles at high RH follow the upper side for decreasing RH and stay liquid until the ambient RH falls below the CRH (Figure 1). The treatment of mixed solutions has further complications. For example, aqueous particles of $X = 0.9$ have a CRH of 32% and form a combination of AS and LET upon crystallization [*Martin et al.*, 2003; *Schlenker et al.*, 2004; *Schlenker and Martin*, 2005].

[4] The complex hysteresis behavior of sulfate phase transitions has not been addressed in previous chemical transport models (CTMs) and SDCF calculations, which instead relied on simplified approaches and limiting cases:

[5] 1. Sulfate particles were assumed to have only one phase in a given model grid box, and the CRH and DRH were set equal to one another to remove the hysteresis bifurcation. *Kiehl et al.* [2000] and *Adams et al.* [2001] assumed that all sulfate particles were in the aqueous

phase (i.e., CRH = DRH = 0). In other studies, limiting cases of (1) DRH = CRH = 35% and (2) CRH = DRH = 80% were used for an assumed composition of ammonium sulfate ($X = 1$) to bracket the uncertainty of the SDCF, found to be 18% in *Boucher and Anderson* [1995] and 14% in *Haywood et al.* [1997].

[6] 2. The relative concentrations of solid and aqueous sulfate particles, coexisting as external mixtures in each model grid box, were estimated based upon local X and RH using thermodynamic models [*Ghan et al.*, 2001; *Martin et al.*, 2004]. The RH history of the particles and hence the hysteresis effect were not explicitly considered. *Martin et al.* [2004] found that solids contributed up to 45% of the tropospheric sulfate mass, and the annual global average SDCF was 25% smaller than a calculation assuming that all particles were aqueous (i.e., CRH = DRH = 0).

[7] As an alternative to using a CTM, *Colberg et al.* [2003] accounted explicitly for the hysteresis effect using RH back trajectory analysis from a Lagrangian model. They also accounted for the global distribution of X values. They found a similar percentage of solids as *Martin et al.* [2004], although the main solid was LET compared to AS of *Martin et al.* [2004], presumably reflecting differences in the global

Table 1. Aerosol Optical Properties at 0.55 μm for Different Aerosol Composition and Relative Humidity (RH)[a]

	5% RH					80% RH				
	m_r[b]	ρ[c]	r_{eff}[d]	E[e]	$\overline{\beta}$[f]	m_r	ρ	r_{eff}	E	$\overline{\beta}$
AS	1.53	1.76	0.17	5.31	0.25	1.41	1.30	0.24	13.28	0.18
AHS	1.47	1.78	0.17	3.95	0.24	1.38	1.31	0.25	11.81	0.17
LET	1.51	1.83	0.17	4.55	0.25	1.40	1.31	0.25	12.71	0.17
SA	1.84	1.84	0.17	3.48	0.22	1.37	1.24	0.30	15.80	0.16
Water	1.33	1.00								

[a]Optical properties are shown for $(NH_4)_2SO_4$ (AS), NH_4HSO_4 (AHS), $(NH_4)_3H(SO_4)_2$ (LET), and H_2SO_4 (SA) particles at 5% and 80% RH. At 5% RH, the properties of AS, AHS, and LET are shown for solids; SA is aqueous. At 80% RH, all particles are aqueous.
[b]Real part of refractive index.
[c]Mass density (g cm^{-3}).
[d]Effective radius (μm).
[e]Mass extinction efficiency (E, (m^2 (gSO$_4^{2-}$)$^{-1}$).
[f]Time-averaged upward backscattered fraction from sunrise to overhead sun. $\overline{\beta}$ can be approximated as $1/2 - 7/16\ g$, where g is the asymmetry factor widely used in radiative transfer models [*Wiscombe and Grams*, 1976].

annual average of X between the two models associated with differences in ammonia emissions. *Colberg et al.* [2003] conducted no SDCF calculations.

[8] We herein treat the hysteresis of the sulfate-ammonium phase transition by explicitly transporting the three solid sulfates, as well as aqueous ammonium and sulfate, and modeling their phase transitions in the GEOS-Chem global CTM [*Park et al.*, 2004], as described in detail by *Wang et al.* [2008]. In brief, different tracers are assigned to represent the different solid and aqueous species. The effect of the RH history on the phase transition (i.e., the hysteresis effect) is modeled in the Eulerian framework by interconverting solid and aqueous species in each model time step according to the CRH and DRH values. At intermediate RH values, solid and aqueous tracers can therefore coexist at a single grid location. In addition, the model of *Wang et al.* [2008] includes partial to complete neutralization of sulfate by ammonia and a composition-dependent treatment of CRH and DRH values. The presently described study extends *Wang et al.* [2008] by modeling SDCF with an explicit account of the variation of aerosol optical properties caused by hysteresis. To assist the analysis of our 3-D model results, in section 2 we first use a column model to illustrate the dependence of the SDCF on the phase of sulfate particles, with emphasis on identifying the key parameters for estimating the SDCF uncertainty. Section 3 describes the methodology of the global model. Sections 4 and 5 present the main results and sensitivity studies, respectively. Conclusions are presented in section 6.

2. Column Study of the Sensitivity of Sulfate Direct Climate Forcing to Particle Phase

[9] For purely scattering particles in an optically thin layer, the sensitivity of the SDCF to particle phase can be analyzed using a column model, as follows [*Wiscombe and Grams*, 1976; *Charlson et al.*, 1992]:

$$SDCF = -A\left(\overline{\beta}_{sd}\tau_{an\_sd} + \overline{\beta}_{aq}\tau_{an\_aq}\right) \qquad (1)$$

where A accounts for such factors as the solar constant, the surface albedo, the cloud fraction, and the atmospheric

transmittance; $\overline{\beta}$ is the time-averaged fraction of solar irradiance scattered backward to space by the aerosol layer; τ is the aerosol optical thickness; the subscript *an* represents the contribution by anthropogenic particles; and the subscripts *sd* and *aq* denote solid and aqueous particles, respectively. Annually and globally averaged, A is approximately 115 W m^{-2} [*Charlson et al.*, 1992]. Application of equation (1) to atmospheric sulfate particles is appropriate because their single-scattering albedo (ω) is nearly 1.00 in the visible region of the spectrum, regardless of phase changes and hygroscopic growth [*Nemesure et al.*, 1995; *Boer et al.*, 2007a, 2007b].

[10] A typical optical thickness for use in equation (1) can be estimated as follows:

$$\tau_{an} = \tau_{an\_sd} + \tau_{an\_aq} = E_{sd}B_{an\_sd} + E_{aq}B_{an\_aq} \qquad (2)$$

where B is the globally averaged sulfate burden ((gSO$_4^{2-}$) m^{-2}) and E is the mass extinction efficiency (m^2 (gSO$_4^{2-}$)$^{-1}$). Both B and E are different for solid and aqueous particles, as denoted by subscripts *sd* and *aq*. The optical thickness is evaluated at 0.55 μm [*IPCC*, 2001, 2007], a wavelength at which the solar flux is representative of the mean across the solar spectrum [*Charlson et al.*, 1992]. For comparison with *IPCC* [2001, 2007], a best estimate of 1.6 mg m^{-2} for B_{an} (i.e., $B_{an\_sd} + B_{an\_aq}$) is adopted here.

[11] The mass extinction efficiency E (m^2 (gSO$_4^{2-}$)$^{-1}$) is calculated for a particle number size distribution $n(r_{dry})$ as follows:

$$E = \frac{3}{4\rho_{dry}}\frac{\int n(r_{dry}, G_r)Q(r_{dry}, G_r)r^2 dr}{\chi_{SO_4}\int n(r_{dry})r_{dry}^3 dr_{dry}} \qquad (3)$$

where G_r is the RH-dependent hygroscopic growth factor (unity for solid particles); Q is the Lorenz-Mie geometric extinction efficiency; ρ_{dry} is the dry particle density (g cm^{-3}); and χ_{SO_4} is the mass fraction of SO$_4^{2-}$ in dry sulfate particles. In this study, ρ_{dry} and G_r follow *Tang* [1996] and include a dependence on X [*Tang and Munkelwitz*, 1994] (see also Table 1). Refractive indices of the aqueous particles are calculated for variable RH using a mole-fraction mixing rule [*Wang and Martin*, 2007].

[12] A lognormal distribution of $n(r_{dry})$ with a geometric mean radius (r_g) of 0.07 μm and a geometric standard deviation (σ_g) of 1.8 is assumed [*Hess et al.*, 1998], rendering an effective radius (r_{eff}) of 0.17 μm and an effective variance (v_{eff}) of 0.41. *Hansen and Travis* [1974] showed that the scattering properties of atmospherically plausible size distributions of spherical particles depend primarily on r_{eff} and v_{eff}. Larger values of r_{eff} or v_{eff} lead to greater values of E_{sd}, and E_{sd} is more sensitive to a variation of r_{eff} than to a variation of v_{eff} [*Kiehl and Briegleb*, 1993]. For sulfate particles, most past studies (see discussion by *Adams et al.* [1999]) assume $r_g = 0.05$ μm and $\sigma_g = 2.0$, which yield the same r_{eff} as this study but a different v_{eff} (0.62). Field measurements show that σ_g is usually less than 2 for accumulation-mode particles [*Wang et al.*, 2003]. For aqueous particles of $X = 1$, the calculated E_{sd} is 5.31 m^2 (gSO$_4^{2-}$)$^{-1}$, and E_{aq}/E_{sd} depends on ambient RH, varying from 1.2 at 40% RH to 2.7 at 80% RH (Figure 2a). The enhancement of E_{aq} arises from the 50% increase of particle radius and

the 10% increase of the geometric extinction efficiency (Figure 2a).

[13] Equation (1) further requires the time-averaged backscattered fraction ($\overline{\beta}$) of solar irradiance by the aerosol layer, calculated as the μ-weighted average of $\beta(\mu)$ from sunrise

to local noon, where μ is the cosine of solar zenith angle. $\beta(\mu)$ is the portion of solar irradiance scattered by the aerosol layer into the upward hemisphere relative to the local horizon. $\beta(\mu)$ varies from less than 0.1 for overhead sun to 0.5 at sunrise (Figure 2b), regardless of particle phase. However, $\overline{\beta}_{aq}/\overline{\beta}_{sd}$ decreases from 0.85 at 50% RH to 0.70 at 80% RH because aqueous particles are larger and therefore have smaller backward scattering.

[14] Equations (1) and (2) taken together show that the product $\overline{\beta}E$ is the key intensive quantity that links sulfate mass to SDCF. Among AS, LET, and AHS, $\overline{\beta}_{sd}E_{sd}$ varies by up to 35%. AS has the largest value because of its high refractive index and small mass density. For aqueous particles, $\overline{\beta}_{aq}E_{aq}$ depends less on particle composition. It is largest for aqueous particles of $X = 0$, followed by $X = 1$, $X = 0.75$, and $X = 0.5$. This ordering is explained first by the large G_r of SA and second by the high refractive index of SA (Table 1 and Figure 2c).

[15] Calculations using equations (1) and (2) for $X = 1$, 80% RH, $B_{an\_aq} = B_{an}$, and $B_{an\_sd} = 0$ (i.e., all aqueous particles) yield an SDCF of -0.43 W m^{-2} (Figure 3). The SDCF decreases by 50% for a contrary assumption of all solid particles (i.e., $B_{an\_aq} = 0$ and $B_{an\_sd} = B_{an}$). In relation to these contrasting cases, *Martin et al.* [2004] estimated an upper limit for B_{an_sd}/B_{an} of 0.45 as a global average by assuming complete lower side behavior in the CTM simulation. The corresponding SDCF in Figure 3 is -0.34 W m^{-2} for $X = 1$. The difference between -0.43 for one limit of $B_{an\_sd}/B_{an} = 0$ and -0.34 W m^{-2} for the other limit of $B_{an\_sd}/B_{an} = 0.45$ represents an uncertainty of 20%, which is close to the 25% uncertainty indicated by *Martin et al.* [2004] for their CTM simulation including variability in X and RH. The uncertainty of 20% obtained in our column model calculation is insensitive to X but decreases to 15% if we assume a global average RH of 60% instead of 80%.

3. Methodology for Global Modeling of Sulfate Phase and Forcing

[16] We use a sulfate-ammonium simulation with the GEOS-Chem CTM driven by assimilated meteorological data for 2001 from the Goddard Earth Observation System (GEOS-3) of the NASA Global Modeling and Data Assimilation Office (GMAO) [*Park et al.*, 2004]. The original data have $1° \times 1°$ horizontal resolution, but for the present
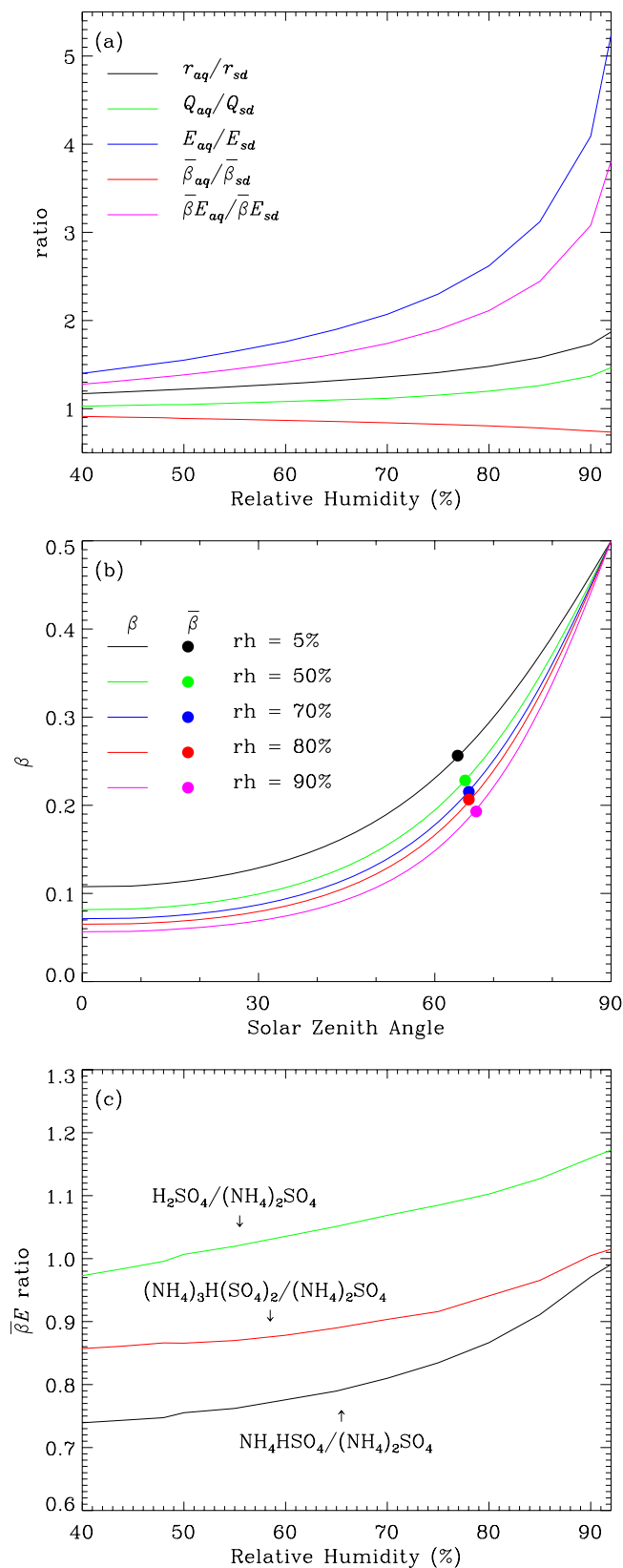
Figure 2. (a) Ratio of the values of the optical properties r, Q, E, $\overline{\beta}$, and $\overline{\beta}E$ of aqueous particles (denoted with subscript aq) for increasing RH to the corresponding values of solid particles (denoted with subscript sd) for $X = 1$. See section 2 of the text for a further explanation of these quantities and the parameters used in the calculation. (b) Backscattered fraction β of radiation to space as a function of the solar zenith angle at different RH values for particles of $X = 1$ along the upper side of the hysteresis loop (CRH = 35%). The daytime averaged backscattered fractions $\overline{\beta}$ from sunrise to sun overhead at the equator. (c) Ratio of $\overline{\beta}E$ values of aqueous particles of H_2SO_4 ($X = 0$), NH_4HSO_4 ($X = 0.5$), and $(NH_4)_3H(SO_4)_2$ ($X = 0.75$) particles to those of $(NH_4)_2SO_4$ ($X = 1$) for increasing RH.
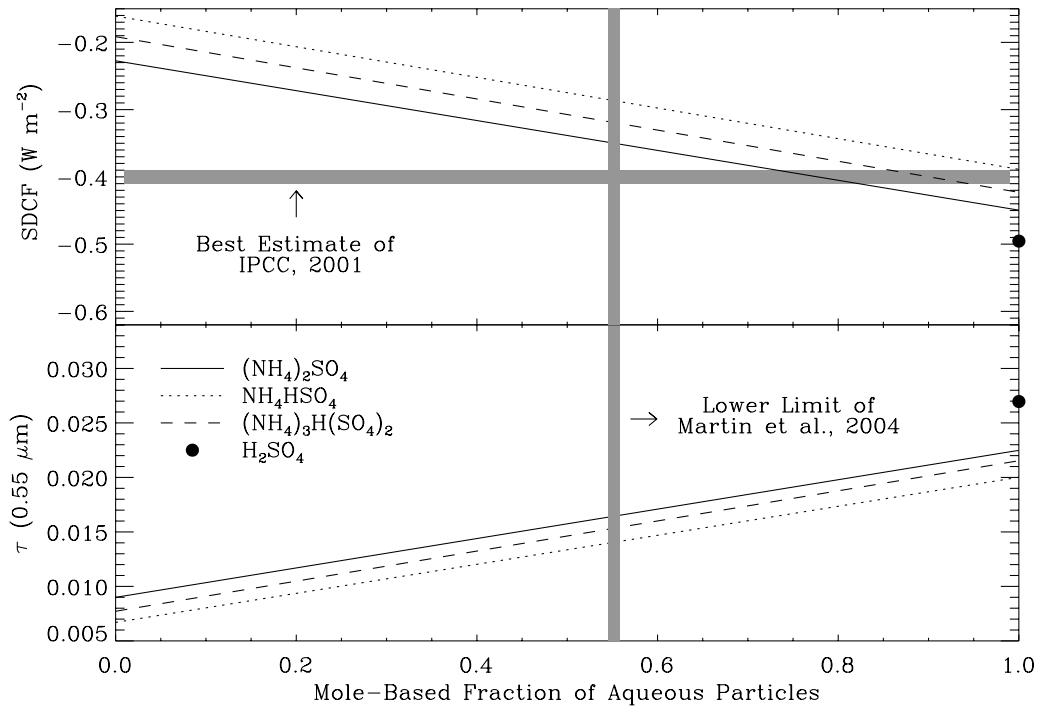
Figure 3. Sulfate direct climate forcing (SDCF) and anthropogenic sulfate aerosol optical thickness (τ_{an}) calculated from a column model for an increasing fraction of aqueous particles. Lines represent different assumptions for the sulfate composition: NH_4HSO_4 (dotted lines), $(NH_4)_3H(SO_4)_2$ (dashed lines), and $(NH_4)_2SO_4$ (solid lines) (i.e., $X = 0.5$, 0.75, and 1.0, respectively). For reference, dots show the results for aqueous H_2SO_4 particles (i.e., $X = 0.0$), which do not have a corresponding solid phase at 298 K. The horizontal gray line represents the current best estimate of the SDCF (-0.4 W m^{-2}) by both IPCC's third [*IPCC*, 2001] and fourth report [*IPCC*, 2007]. The vertical gray line represents the lower limit estimate of aqueous sulfate fraction (55%) calculated by *Martin et al.* [2004]. In the calculations of Figure 3, the optical properties of aqueous particles are taken at RH = 80%, although this RH value exceeds the DRH values of the solids. The anthropogenic sulfate column burden is 1.6 mg m^{-2}, which is the same value used by *IPCC* [2001].

simulation we degrade this resolution to $4° \times 5°$ for computational expediency. Sulfur and ammonia emission inventories are the same as those given by *Park et al.* [2004] and *Martin et al.* [2004].

[17] The method used for simulating the phase transitions of sulfate-ammonium particles is detailed by *Wang et al.* [2008]. We transport explicitly the different sulfate forms (namely, AS, LET, AHS, and aqueous) and track the RH history of the particles and hence the hysteresis loop within the Eulerian framework. We use DRH_0 values for AHS, LET, and AS of 42%, 69%, and 80%, respectively [*Martin*, 2000]. The subscript "0" indicates a reference value as measured in the laboratory. CRH_0 values of aqueous sulfate particles are determined locally according to the extent of ammonium neutralization (X) [*Martin et al.*, 2003]:

$$CRH_0(X) = -71925 + 1690X - 139X^2 + \frac{1770760}{25 + 0.5(X - 0.7)} \quad (4)$$

The temperature dependence of the DRH and the CRH, which is minor at least for $X = 1$, is neglected [*Onasch et al.*, 1999].

[18] A four-stream broadband radiative transfer model (RTM), employing monthly mean surface reflectance data [*Koelemeijer et al.*, 2003] and the simulated 3-D aerosol sulfate mass and partitioning, is employed for the forcing calculations [*Fu and Liou*, 1993; *Wang et al.*, 2004]. The RTM is applied to the solar spectrum for six bands, ranging from 0.2 to 4 μm. Band averages of X- and RH-dependent optical properties (e.g., ω, β, Q, E, and asymmetry parameter g) are tabulated in the RTM for computational expediency. The difference between upwelling solar irradiances calculated in the presence compared to the absence of sulfate aerosols is the clear-sky sulfate direct radiative effect, which is then reduced by the cloud fraction (C_f) to yield the full-sky value. *Haywood et al.* [1997] and *Penner et al.* [1998] independently showed that the contribution of forcing in cloudy regions to the global SDCF is less than 4%. The global mean C_f of GEOS-3 is 0.63, and *Liu et al.* [2006] showed that GEOS-3 cloud fields are in good agreement with satellite observations. For computational expediency, the forcing calculation in each grid box is conducted hourly for a 24-h time period on the middle day of each month using the monthly averaged aerosol optical thickness calculated for every 30 min during the entire month [*Yu et al.*, 2006].

[19] Model simulations are conducted with a 4-month spin-up for the year 2001 using emission scenarios that include and exclude anthropogenic SO_2 and NH_3. In each
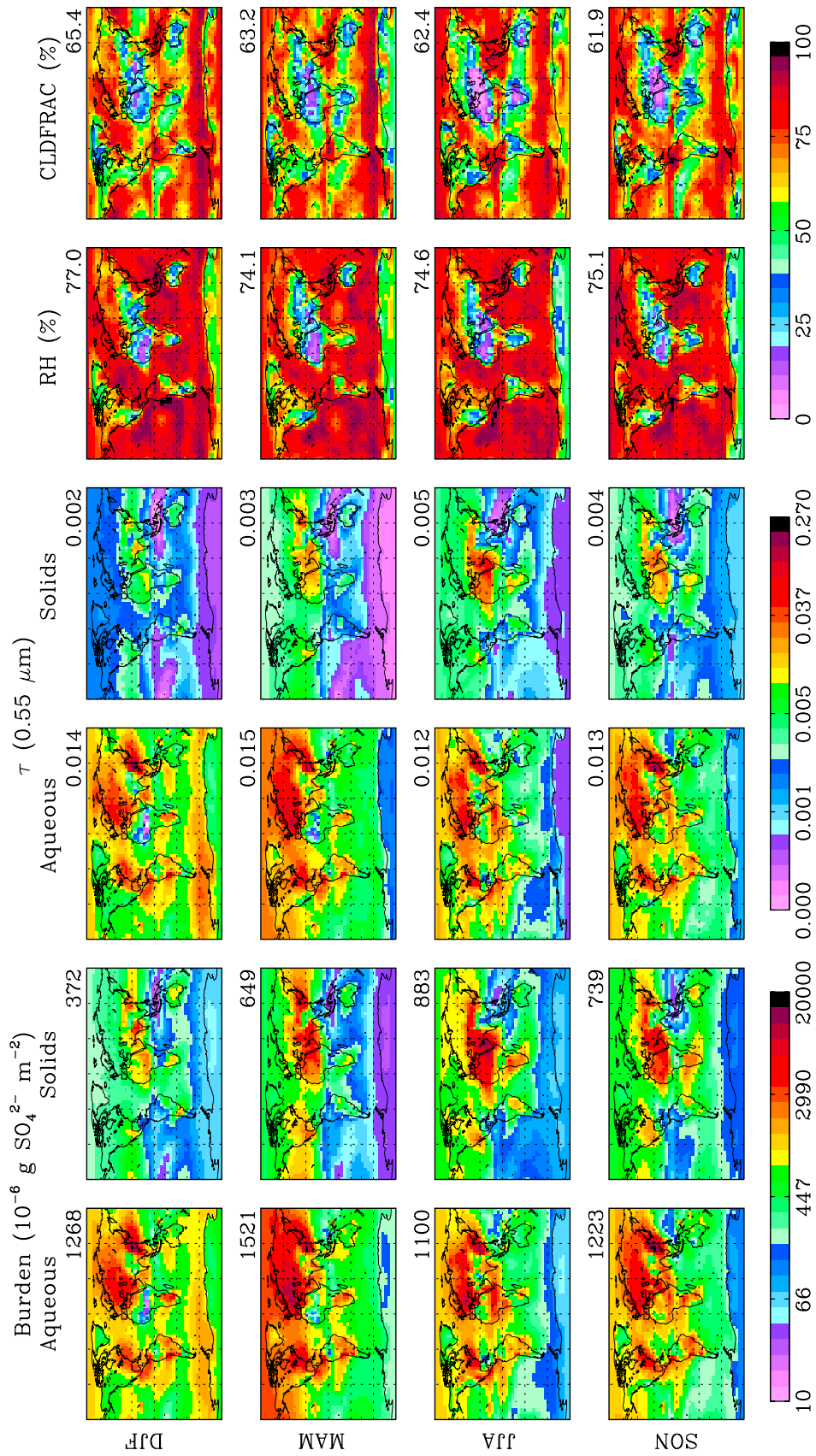
Figure 4. Seasonal and geographic distributions of tropospheric sulfate burdens (natural + anthropogenic) in aqueous and solid phases, the corresponding sulfate aerosol optical thickness τ_{aq} and τ_{sol}, the average relative humidity (RH) in the boundary layer, and the cloud fraction of the column (CLDFRAC). The numbers located to the upper right of each panel show globally averaged quantities.
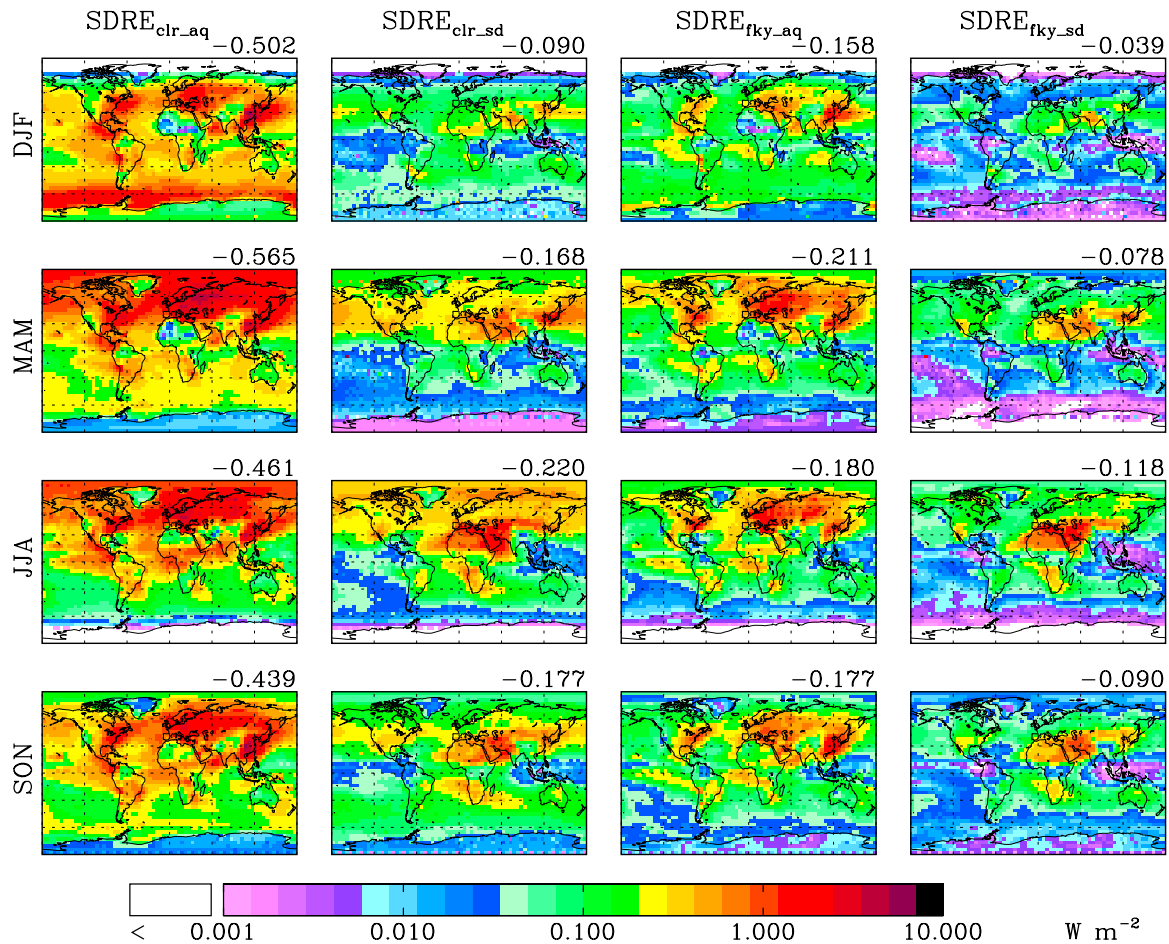
Figure 5. Seasonal and geographic distributions of the clear-sky sulfate direct radiative effect of aqueous ($SDRE_{clr\_aq}$) and solid ($SDRE_{clr\_sd}$) particles as well as their full-sky counterparts $SDRE_{fky\_aq}$ and $SDRE_{fky\_sd}$ that include the effects of cloud fraction.

emission scenario, four simulations are conducted, including one base case simulation with full accounting of the composition-dependent hysteresis loop as well as cases that omit hysteresis by assuming that (1) CRH = DRH = 0, (2) CRH = DRH_0, or (3) DRH = CRH_0 (Figure 1). Although case 3 is not consistent with theory or experiment (i.e., deliquescence does not occur at the CRH), earlier studies have employed it as a heuristic approach for omitting hysteresis from model simulations. (For clarity to the reader, case 2 denoted for brevity herein as CRH = DRH_0 is the same as CRH = DRH* in Table 1 of *Wang et al.* [2008], which is explained therein at length.)

4. Base Case Results With Consideration of Hysteresis Loop

4.1. Sulfate Direct Radiative Effect

[20] The geographic distributions of aqueous and solid sulfate burdens for the base case, including both natural and anthropogenic emissions, are shown in Figure 4 (left) for the four seasons. Global average burdens are 1.64, 2.17, 1.98, and 1.96 mg m^{-2} in DJF, MAM, JJA, and SON, respectively. This seasonal variation agrees well with pre-

vious studies [*Koch*, 2001; *Martin et al.*, 2004]. Global B_{sd}/B ranges from 23% in DJF to 45% in JJA, as explained by the greater neutralization of the sulfate particles in the summer in the model [*Wang et al.*, 2008].

[21] Global distributions of τ_{aq} and τ_{sd} have similar patterns as B_{aq} and B_{sd}, respectively (Figure 4, middle). The seasonal variation of τ_{aq} is less than 10%, with a maximum of 0.015 in MAM, a minimum of 0.012 in JJA, and an annual average of 0.0135. In contrast, τ_{sd} has a seasonal variation of more than 100%, with a maximum of 0.005 in JJA, a minimum of 0.002 in DJF, and an annual average of 0.0035. As a result, τ_{sd}/τ is 29% in JJA but 13% in DJF, with an annual average of 20%.

[22] The global annual clear-sky SDRE ($SDRE_{clr}$) and full-sky SDRE ($SDRE_{fky}$) are shown in Figure 5 for aqueous and solid particles for the four seasons. Overall, $SDRE_{fky}$ = −0.263 W m^{-2} (Table 2), with a maximum in JJA (−0.3 W m^{-2}) and a minimum in DJF (−0.19 W m^{-2}). Furthermore, $SDRE_{fky}/SDRE_{clr}$ = 40%, which partitions as $SDRE_{fky\_sd}/SDRE_{clr\_sd}$ = 55% for solids compared to $SDRE_{fky\_aq}/SDRE_{clr\_aq}$ = 35% for aqueous particles. The relative enrichment for solids occurs because they are associated with dry conditions

Table 2. Global Annual Averages of Natural Plus Anthropogenic Sulfate Burden (B), Aerosol Optical Thickness (τ), and Clear-Sky and Full-Sky Sulfate Direct Radiative Effects (i.e., SDRE$_{clr}$ and SDRE$_{fky}$) for the Different Cases Described in the Text[a]

	CRH = DRH = 0, "All Aqueous"	DRH = CRH$_0$, "Upper Side"	Base Case	CRH = DRH$_0$, "Lower Side"	Base Case, $g_{aq} = g_{sd}$[b]	Base Case, $X = 1$[c]	DRH = CRH$_0$, $X = 1$	DRH = CRH$_0$, $X = 1$, $g_{aq} = g_{sd}$
B (mg SO$_4^{2-}$ m^{-2})								
Total	1.932	1.931	1.940	1.947	1.940	1.943	1.934	1.934
% solids[d]	0.0%	17.1%	34.1%	56.0%	34.1%	40.2%	22.0%	22.0%
$\tau \times 10^4$ at 0.55 μm								
Total	183	177	170	153	170	165	175	175
% solids	0.0%	9.7%	20.3%	37.1%	20.3%	24.7%	12.7%	12.7%
SDRE$_{clr}$ (W m^{-2})								
Total	0.687	0.672	0.656	0.608	0.787	0.691	0.716	0.861
% solids	0.0%	11.8%	25.0%	43.5%	20.8%	28.4%	14.6%	12.2%
SDRE$_{fky}$ (W m^{-2})								
Total	0.278	0.270	0.263	0.245	0.307	0.277	0.288	0.338
% solids	0.0%	15.8%	34.1%	52.0%	26.5%	34.5%	19.0%	16.2%
% ratio to base case								
τ	107.6%	104.1%	n/a	90.0%	n/a	97.1%	102.9%	102.9%
SDRE$_{fky}$	105.7%	102.7%	n/a	93.2%	116.7%	105.3%	110.0%	128.5%

[a]The dependence of CRH, DRH, and aerosol optical properties on composition X is included in the calculations unless otherwise noted.
[b]Same as the base case except that the asymmetry parameter of solid particles is also employed for aqueous particles.
[c]All sulfate particles are fully neutralized (i.e., ammonium sulfate).
[d]Shows the percent contribution by solids to the indicated total (i.e., B, τ, SDRE$_{clr}$, or SDRE$_{fky}$).

and are thus anticorrelated with clouds. The relative contribution of solid particles to full-sky SDRE (i.e., SDRE$_{fky\_sd}$/SDRE$_{fky}$ = 34%) is thus larger than one would expect simply from optical thickness (i.e., τ_{sd}/τ = 20%).

4.2. Sulfate Direct Climate Forcing

[23] The geographic distributions of anthropogenic sulfate aerosol optical thickness for aqueous and solid particles (τ_{an_aq} and τ_{an_sd}, respectively) are shown in Figure 6 (left) for the four seasons. Globally and seasonally averaged, the anthropogenic contribution (0.010) is 60% of the total. τ_{an} can be as high as 0.4 over industrial regions of Europe, North America, and east Asia. It can also be as low as 0.002 over remote regions. Large τ_{an_sd} occurs over the Sahel in JJA because of transport from Europe. The fractional contribution of solids (τ_{an_sd}/τ_{an}) is greatest in JJA (36%) and lowest in DJF (16%), with an annual average of 26% (Figure 6, middle). The seasonal variation is explained by the greater neutralization of particles in JJA, resulting in higher CRH values and consequently greater solids mass fractions. Greater neutralization in JJA is caused by the warmer temperatures over the Northern Hemisphere and greater biomass burning over the Southern Hemisphere [*Wang et al.*, 2008], both of which lead to higher NH$_3$ emissions.

[24] The full-sky SDCF (SDCF$_{fky}$), which by definition includes only anthropogenic aerosols, is shown in Figure 6 (right). The SDCF$_{fky}$ reaches its maximum in JJA (-0.20 W m^{-2}) and minimum in DJF (-0.11 W m^{-2}). The quantity SDCF$_{fky}$/SDCF$_{clr}$ = 44% partitions as SDCF$_{fky\_sd}$/SDCF$_{clr\_sd}$ = 51% and SDCF$_{fky\_aq}$/SDCF$_{clr\_aq}$ = 40% for solid and aqueous particles, respectively, again indicating the anticorrelation of solid particles with cloud-free conditions. This anticorrelation and the larger backscattering fraction of solid particles together imply that the solid particles make a contribution to forcing that is disproportionately higher than expected from optical thickness alone (i.e., SDCF$_{fky\_sd}$/SDCF$_{fky}$ = 37% compared to τ_{an_sd}/τ_{an} = 26%). As a global

average, SDCF$_{fky\_sd}$/SDCF$_{fky}$ has a maximum of 47% in JJA and a minimum of 26% in DJF. Anthropogenic solid particles also make a slightly greater contribution than their natural solid counterparts (i.e., SDCF$_{fky\_sd}$/SDCF$_{fky}$ = 37% compared to SDRE$_{fky\_sd}$/SDRE$_{fky}$ = 34%).

4.3. Comparison With Other Studies

[25] The simulated seasonal variations and geographical distributions of B, B_{an}, τ, τ_{an}, SDRE, and SDCF in this study are in qualitative agreement with earlier studies [e.g., *Koch et al.*, 1999; *Kiehl et al.*, 2000; *Ghan et al.*, 2001; *Martin et al.*, 2004]. Quantitatively, however, the global annual averages of this study are lower. For example, the results from nine different CTMs having the same emission inventories, as carried out during the AeroCOM project (Aerosol Comparisons between Observations and Models), give B_{an}, τ_{an}, and SDCF as 2.12 ± 0.82 mg m^{-2}, 0.019 ± 0.009, and -0.35 ± 0.15 W m^{-2}, respectively, expressed as mean±standard deviation [*Schulz et al.*, 2006]. The corresponding values obtained here for the base case are 1.25 mg m^{-2}, 0.010, and -0.17 W m^{-2} (Table 3). The lower values of our study can be attributed in large part to differences in the emission inventories of sulfur, given as 98 Tg/a in AeroCom [*Dentener et al.*, 2006] and 73 Tg/a in this study. The lower value of the SDCF in our study is also partially attributable to differences in aerosol optical properties (see section 5.3) and the omission of SDCF calculations for cloudy regions.

[26] In model intercomparisons of aerosol forcing, a standard practice is to calculate both the normalized SDCF (which is SDCF/B_{an} and denoted hereafter as NSDCF) and the global-normalized mass extinction efficiency (i.e., $NE = \tau_{an}/B_{an}$). Quantities NSDCF and NE serve as an approach for minimizing the impact of model differences in emission inventories and meteorology and thereby allowing a focus on aerosol optical properties and radiative transfer [*Boucher and Anderson*, 1995; *Kinne et al.*, 2006]. The NSDCF and NE values for the present study are -136 W (gSO$_4^{2-}$)$^{-1}$ and
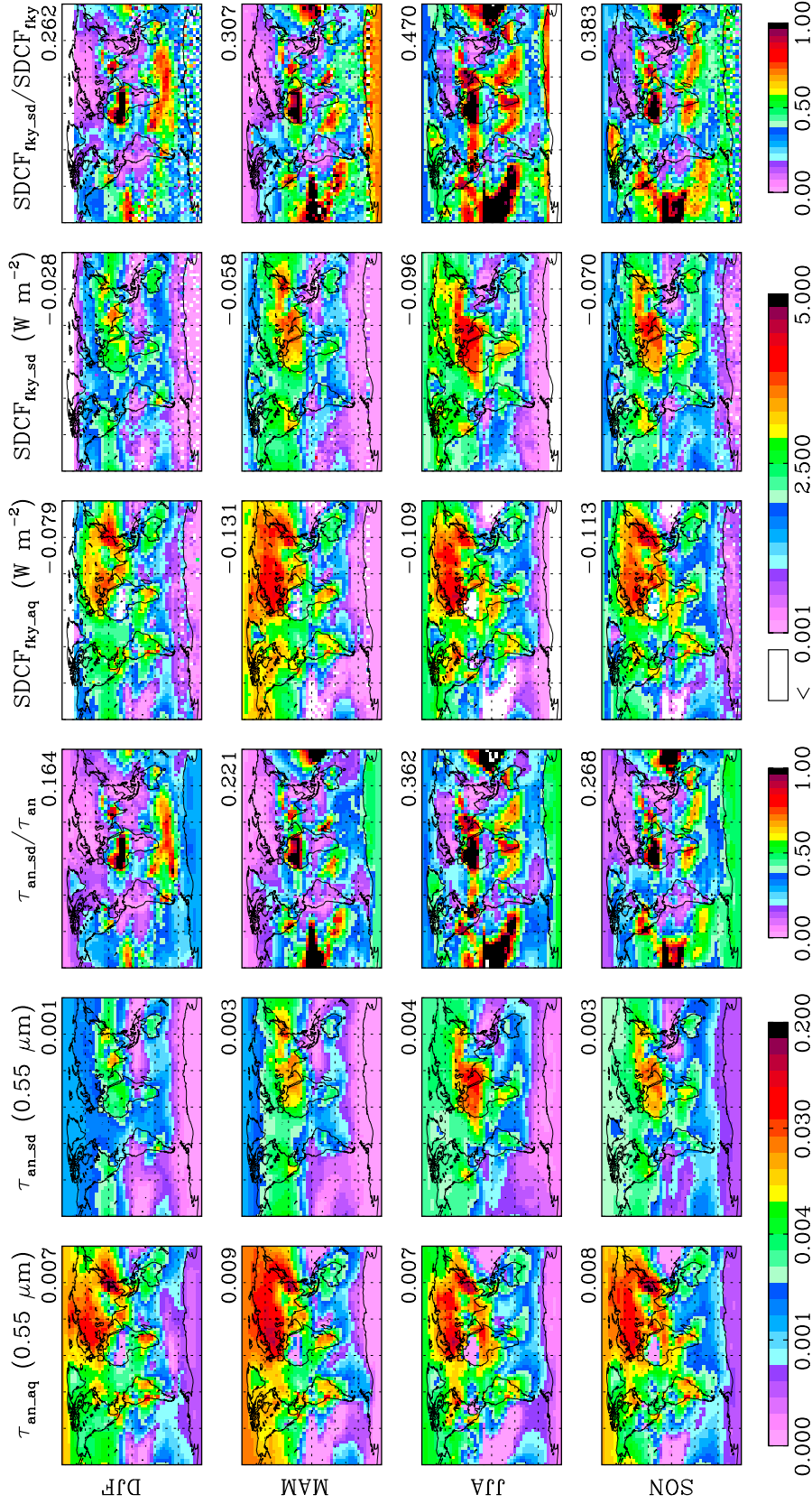
Figure 6. Seasonal and geographic distributions of anthropogenic sulfate aerosol optical thickness for aqueous (τ_{an_aq}) and solid particles (τ_{an_sd}) as well as the fractional contribution by anthropogenic solids τ_{an_sd}/τ_{an}. Also shown are the corresponding full-sky sulfate direct radiative forcings SDCF$_{fky\_aq}$ and SDCF$_{fky\_sd}$ as well as the fractional contribution by solids SDCF$_{fky\_sd}$/SDCF$_{fky}$.

Table 3. Global Annual Averages of Anthropogenic B_{an}, τ_{an}, $SDCF_{clr}$, and $SDCF_{fky}$ Calculated for the Sensitivity Studies Described in the Text[a]

	CRH = DRH = 0, "All Aqueous"	DRH = CRH$_0$, "Upper Side"	Base Case	CRH = DRH$_0$, "Lower Side"	Base Case, $g_{aq} = g_{sd}$[b]	Base Case, $X = 1$[c]	DRH = CRH$_0$, $X = 1$[c]	DRH = CRH$_0$, $X = 1$, $g_{aq} = g_{sd}$
B_{an} (mg SO$_4^{2-}$ m^{-2})								
Total	1.239	1.241	1.247	1.254	1.247	1.251	1.239	1.239
% solids[d]	0.0%	20.8%	40.6%	67.6%	40.6%	49.2%	22.4%	22.4%
$\tau_{an} \times 10^4$ at 0.55 μm								
Total	113	108	103	90	103	101	108	108
% solids	0%	11.6%	26.2%	47.2%	26.2%	31.9%	15.6%	15.6%
$SDCF_{clr}$ (W m^{-2})								
Total	0.411	0.404	0.389	0.359	0.455	0.404	0.422	0.501
% solids	0%	14.7%	31.4%	56.1%	26.9%	37.5%	18.1%	15.3%
$SDCF_{fky}$ (W m^{-2})								
Total	0.184	0.178	0.170	0.157	0.195	0.176	0.184	0.214
% solids	0.0%	19.0%	36.8%	63.4%	32.3%	43.0%	22.5%	19.3%
% to base case								
τ_{an}	109.7%	104.9%	n/a	85.4%	n/a	98.1%	104.9%	104.9%
$SDCF_{fky}$	108.2%	104.7%	n/a	92.4%	114.7%	103.5%	108.2%	125.9%

[a]The dependence of CRH, DRH, and aerosol optical properties on composition X is included in the calculations unless otherwise noted.
[b]Same as the base case except that the asymmetry parameter of solid particles is also employed for aqueous particles.
[c]All sulfate particles are fully neutralized (i.e., ammonium sulfate).
[d]Shows the percent contribution by solids to the indicated total (i.e., B_{an}, τ_{an}, $SDCF_{clr}$, or $SDCF_{fky}$).

8.35 m^2 g^{-1}, respectively. These values can be compared to -161 ± 41 W $(gSO_4^{2-})^{-1}$ and 9.1 ± 2.7 m^2 g^{-1}, respectively, in the work by *Schulz et al.* [2006]. This study's values are smaller than -261 W$(gSO_4^{2-})^{-1}$ and 11.8 m^2 g^{-1}, respectively, of *Martin et al.* [2004], who omitted the decrease of the real part of the refractive index as a result of hygroscopic growth, in turn rendering an overestimate of E_{aq} in the forcing calculations. *Adams et al.* [2001] showed that omission of composition-dependent aerosol optical properties (i.e., $\overline{\beta}E$) accompanying hygroscopic growth results in a +35% bias of the global SCDF, although their evaluation assumed all aqueous particles.

[27] A complication in model intercomparisons is that differences in NSDCF and *NE* in the compared models can arise, even for the same values of E_{aq} and E_{sd}, because of differing approaches for treating the hysteresis effect. In addition to the NSDCF, we therefore also introduce in this study a recommendation that a complementary measure, namely a globally averaged growth factor of aerosol optical thickness (defined further below in equation (9)), has value for model intercomparisons to normalize for different model treatments (including omissions) of particle phase transitions. Returning to the column models of equations (1) and (2), earlier studies that did not explicitly treat sulfate phase transitions did implicitly assume some weighted average, as follows:

$$SDCF = -A\overline{\beta}'E'B_{an}, \tag{5}$$

where

$$\overline{\beta}'E' = \frac{\overline{\beta}_{sd}E_{sd}B_{an\_sd} + \overline{\beta}_{aq}E_{aq}B_{an\_aq}}{B_{an}}. \tag{6}$$

The prime notation emphasizes the masking of the hysteresis effect.

[28] In earlier studies, $\overline{\beta}'$ of equation (5) was taken as either $\overline{\beta}_{sd}$ [*Charlson et al.*, 1992; *Kiehl and Briegleb*, 1993]

or $\overline{\beta}_{aq}$ [*Kiehl et al.*, 2000]. The resulting bias has never been previously reported to the best of our knowledge. Sections 5.2 and 5.3 return to this topic.

[29] In most past approaches, E' of equation (5) was calculated by applying a growth factor (G') to E_{sd}, as follows:

$$E' = G'E_{sd} \tag{7}$$

for which $\tau_{an} = E'B_{an} = G'E_{sd}B_{an}$. Upon close inspection, however, the approach embedded in equation (7) has some important limitations. To dissect G' into its contributing hysteresis-dependent factors, we substitute and rearrange equation (2), leading to the result:

$$G' = G_E - \frac{B_{an\_sd}}{B_{an}}(G_E - 1) \tag{8}$$

where G_E is the growth factor of the mass extinction efficiency of aqueous particles, given by $G_E = E_{aq}/E_{sd}$. Equation (8) shows that the coexistence of solid and aqueous particles in a column (i.e., $B_{an\_sd}/B_{an} < 1$) implies that $G' < G_E$ and further that G' cannot be accurately calculated without knowledge of B_{an_sd}/B_{an}.

[30] Without calculating B_{an_sd}, earlier studies made assumptions such as $B_{an\_sd} = 0$ (e.g., $G' = G_E$ in the work by *Kiehl et al.* [2000]), $B_{an\_sd}/B_{an} = 0.5$ (e.g., $G' = 1 + 0.5G_E$ in the work by *Chuang et al.* [1997]), or a linear decrease of B_{an_sd}/B_{an} between CRH and DRH (e.g., $G' = 1$ at CRH but then linearly increases with RH to $G' = G_E$ at DRH in the work by *Haywood et al.* [1997]). Other approaches have included parameterizing G' by assuming $G' = 1$ when RH is less than a threshold (such as 60%) and then assuming $G' = G_E$ at higher RH values [*Charlson et al.*, 1992; *Koch et al.*, 1999]. These various approaches for column models highlight first that CTM intercomparisons of SDCF are influenced by how phase transitions are addressed and second that there is a consequent need for
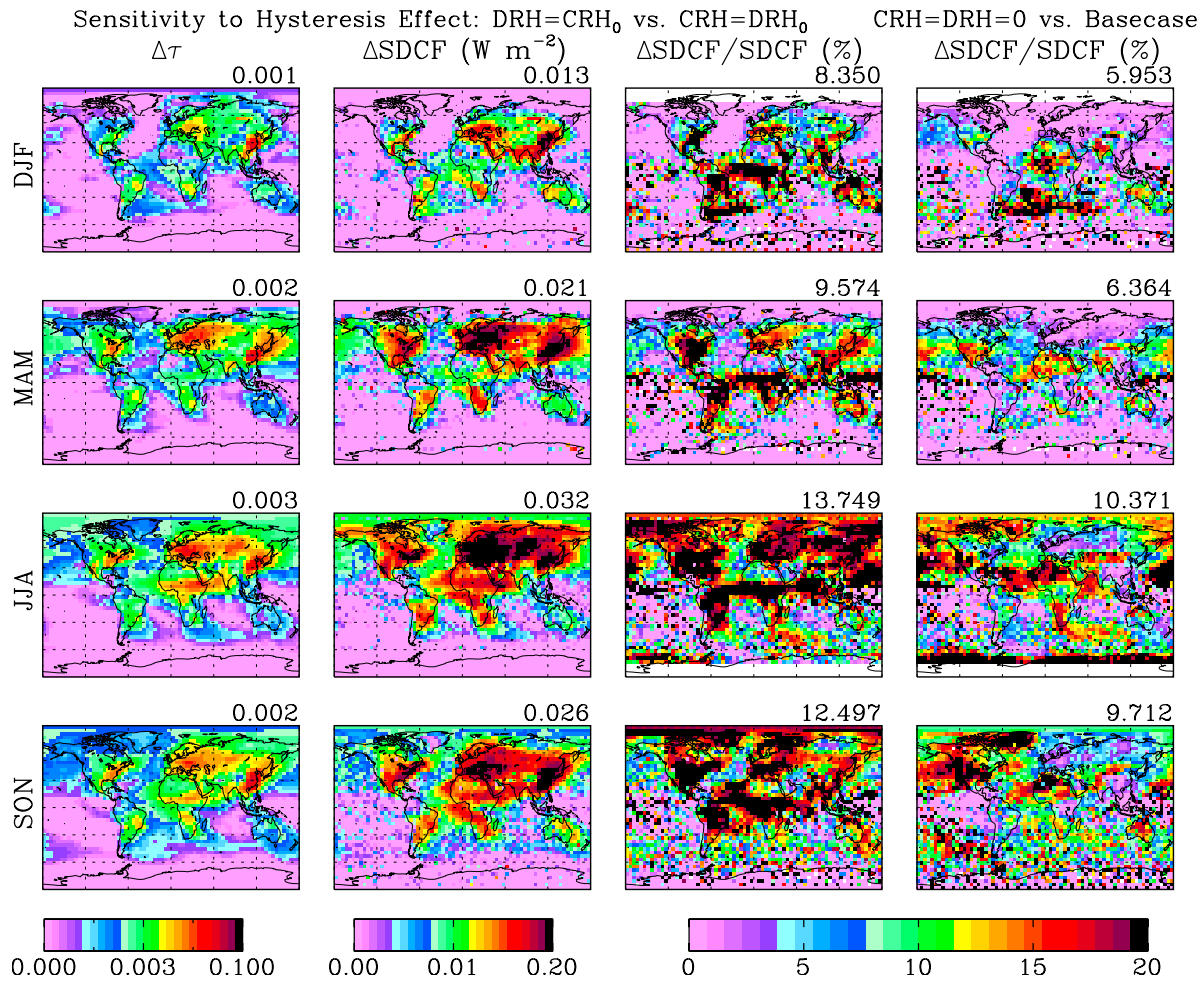
Figure 7. Sensitivity to the hysteresis effect. The first column shows the difference of τ_{an} between the cases of DRH = CRH$_0$ and CRH = DRH$_0$. The second column shows the corresponding difference in the SDCF. The percent ratio of this difference to the SDCF of the base case is shown in the third column. The fourth column shows a similar percent ratio but the numerator is the difference in the SDCF between the case of CRH = DRH = 0 and the base case.

a normalization of the SDCF with respect to the hysteresis effect.

[31] The different CTM treatments of phase transitions can be normalized, with respect to their effects on predicting the SDCF, by intercomparing the normalized growth factors of aerosol optical thickness (NG_τ), calculated as:

$$NG_\tau = \frac{\tau_{an}}{\tau_{an\_all\_sd}} = \frac{\tau_{an}}{E_{sd}\left(B_{an} + B_{aq}\right)} \qquad (9)$$

The quantity $\tau_{an\_all\_sd}$ is the optical thickness assuming that all particles are solid. NG_τ is then the ratio of τ including hygroscopicity to τ omitting it. NG_τ thus quantifies how important are hygroscopic effects and hence imbedded treatments of hysteresis in CTM predictions of the SDCF. Reporting of NG_τ values should therefore facilitate an additional meaningful perspective for understanding differences among the SDCF estimates of different CTMs.

[32] Many CTM studies (such as those in the AeroCom project) did not report $\tau_{an\_all\_sd}$, thus hampering efforts to evaluate the role of differing approaches for treating hys-

teresis to explain differences of the SDCF values among the compared CTMs. Here, we can compare our present results with those of *Koch* [2001], *Martin et al.* [2004], and *Reddy et al.* [2005], who reported E_{sd}, B_{an}, and τ_{an}. The present study also allows variable chemistry. In terms of implementation, the denominator $\tau_{an\_all\_sd}$ in the calculation of NG_τ in equation (9) is obtained as follows. First, the model is run using CRH = DRH = 100% (i.e., all solids). Then, $\tau_{an\_all\_sd}$ is calculated by using composition-dependent E_{sd} values.

[33] The global annual average of NG_τ (1.6) for the base case of our study is comparable to the value of 1.7 of *Koch* [2001] but about 30% smaller than the value of 2.3 of *Reddy et al.* [2005]. Koch assumed that all particles below a threshold value of 60% RH are solids and employed an interpolated growth factor for aqueous sulfate particles. The high NG_τ of *Reddy et al.* [2005] is possibly explained by their use of a low deliquescence-crystallization threshold of 30% RH (i.e., CRH = DRH = 30%), thus overestimating the contribution by aqueous particles. NG_τ values given by *Martin et al.* [2004] varied from 2.6 in the case of CRH = DRH = 0 to 2.0 in the case of CRH = DRH$_0$. These relatively large values arise from the high *NE* values of

Table 4. Comparison of Quantities From This Study to Those in Literature[a]

	B_{an}	$\tau_{an} \times 10^4$	SDCF	NSDCF[b]	NE[c]	NG_τ	r_{eff}[d]	v_{eff}[d]	E_{sd}	E_{aq}[e]	Remarks
Reddy et al. [2005]	3.03	300	−0.41	−135	9.90	2.30	0.12	0.62	4.3	12.1[f]	For RH< 30%, E_{sd} applies. For RH > 30%, Mie−calculated E_{aq} values apply for increasing RH.
Koch et al. [1999], Koch [2001][g]	3.30	280	−0.68	−206	8.48	1.70	0.30	0.20	5.0	11.0	For RH< 60%, E_{sd} applies. For RH > 60%, E_{aq} at 85% RH and E_{sd} are interpolated to obtain E_{aq} at intermediate RH values.
Martin et al. [2004]											
CRH = DRH = 0	1.53	180	−0.40	−261	11.76	2.56	0.13	0.62	4.6	17.7	Refractive index does not vary with RH.
Lower side	1.53	140	−0.34	−222	9.15	2.00	—	—	—	—	—
Schulz et al. [2006][h]											
Mean	2.12	190	−0.35	−161	9.10						Statistics from nine CTMs having the same emissions.
Standard deviation	±0.82	±90	±0.15	±41	±2.70						—
This study[i]							0.17	0.41	3.9–5.3	11.8–15.8	E_{sd} and E_{aq} depend on particle composition X. The hysteresis loop is fully considered in the base case.
CRH = DRH = 0	1.24	113	−0.18	−149	9.12	1.76	—	—	—	—	—
DRH = CRH_0	1.24	108	−0.18	−143	8.70	1.69	—	—	—	—	—
Base case	1.25	103	−0.17	−136	8.26	1.60	—	—	—	—	—
CRH = DRH_0	1.25	90	−0.16	−125	7.17	1.40	—	—	—	—	—
Base case, $g_{aq} = g_{sd}$	1.25	103	−0.17	−156	8.26	1.60	—	—	—	—	—
Base case, $X = 1$	1.25	101	−0.18	−141	8.07	1.57	—	—	—	—	—
DRH = CRH_0, $X = 1$	1.24	108	−0.18	−149	8.72	1.68	—	—	—	—	—
DRH = CRH_0, $X = 1$, $g_{aq} = g_{sd}$	1.24	108	−0.21	−172	8.72	1.68	—	—	—	—	—

[a]Quantities refer to anthropogenic contribution only. Table cells are blank when a value is not available. Units for the various quantities are the same as those given throughout the text.
[b]NSDCF = SDCF/B_{an}.
[c]NE = τ_{an}/B_{an}.
[d]Calculated for the dry aerosol size distribution.
[e]Calculated for 80% RH.
[f]Based upon Figure 1 of *Reddy et al.* [2005].
[g]According to *Koch et al.* [1999] and *Koch* [2001].
[h]This study obtains the average and standard deviation of results of nine CTMs. *NE* is derived from *Kinne et al.* [2006].
[i]This study are derived from Table 3 of this study. Values of r_{eff} and v_{eff} are the same in all cases of this study, and values of E_{sd} and E_{aq} depend on the neutralization of sulfate particles (Table 1).

Martin et al. (see above). These comparisons, as well as the different sensitivity analyses of this study (see section 5), show that different treatments of sulfate phase and water content can result in a variation in NG_τ of approximately 50%. In comparison, a variation of 30–50% is reported in literature for NSDCF and NE values. The parameters NSDCF and NE are therefore in themselves not fully sufficient to isolate the uncertainties in the SDCF that arise from how the hysteresis of particle phase and hence hygroscopicity is treated.

5. Sensitivity Analysis

5.1. Omission of the Hysteresis Loop

[34] The effects on the SDRE and the SDCF for the three approaches considered for omitting the hysteresis of sulfate phase transitions are summarized in Tables 2 and 3. The cases assume that (1) CRH = DRH = 0, (2) CRH = DRH$_0$, and (3) DRH = CRH$_0$ (Figure 1). These have been variously used as simplifying assumptions in earlier studies. The case of CRH = DRH$_0$ leads to the largest differences of τ_{an} and SDCF$_{fky}$ from their base case values (i.e., −15% and −8% respectively, as global and annual averages). For the case of CRH = DRH = 0, these values increase by +10% and +8%, respectively. The case of DRH = CRH$_0$ increases both τ_{an} and SDCF$_{fky}$ by +5%. Therefore, the most divergent model assumptions of CRH = DRH = 0 and CRH = DRH$_0$ result in differences of τ_{an} and SDCF$_{fky}$ of 25% and 16%.

[35] To quantify seasonally and regionally how the treatment of phase transitions can affect the modeled SDCF, we calculate the difference in the SCDF$_{fky}$ between the cases of DRH = CRH$_0$ and CRH = DRH$_0$ and divide this difference by the SCDF$_{fky}$ of the base case. Figure 7 shows this quantity seasonally and regionally and indicates large variability in the sensitivity of the SDCF$_{fky}$ to the treatment of the hysteresis effect. On the low side, the sensitivity is approximately 0% over the remote oceans and less than +5% in coastal ocean regions affected by offshore transport of pollution. On the high side, sensitivities of +10% to +20% occur nearby industrial or arid continental regions. The seasonal uncertainty is largest in JJA, with changes in SDCF$_{fky}$ of +15% for the midlatitude continents excluding Australia. Sensitivities as high as +15% and +20% are apparent over northeastern USA and east Asia, respectively, in JJA. In comparison, the case of CRH = DRH = 0 compared to the base case leads to a bias in SDCF$_{fky}$ of +8% as a global annual average, although the Sahel region in JJA is an important regional outlier (the fourth column of Figure 7), having values as high as +15%.

5.2. Sensitivity to Extent of Neutralization

[36] To evaluate the effect of variable chemical composition (i.e., X) on the SDCF, we modified the base case by assuming that all particles have $X = 1$ (i.e., fully neutralized). This approach underestimates τ_{an} by −2% (Table 3) compared to the base case as a result of two competing factors. (1) The fraction of solids increases by +9% because the CRH has its highest value for $X = 1$. (2) E_{sd} of AS is larger than that of LET and AHS, and $E_{aq}(X; RH)$ is maximum for $X = 1$ (excluding highly acidified conditions). Hence, although τ_{an_sd} is increased by both factors, τ_{an_aq} is decreased by the first factor but increased

by the second. The overall balance of these effects is a −2% change of τ_{an}.

[37] Although τ_{an} decreases, SDCF$_{fky}$ concomitantly increases by 3.5%, explained as follows. (1) The +9% increase in solids raises the overall backscattered fraction because $\overline{\beta}_{sd} > \overline{\beta}_{aq}$. (2) The $\overline{\beta}E$ value increases for both solid and aqueous particles of $X = 1$ compared to those of $X < 1$, excluding highly acidic solutions (Table 1). Hence, in an evaluation of the uncertainty in the SDCF, the effects of sulfate phase and sulfate composition on $\overline{\beta}E$ should be considered, as they can lead to similar SDCF$_{fky}$ but for different reasons, i.e., because of a decrease of $\overline{\beta}$ and an increase of E, on the one hand, or an increase of E and a decrease of $\overline{\beta}$, on the other hand (Tables 2 and 3).

5.3. Sensitivity to Other Factors

[38] Our last sensitivity study, conducted with the purpose of facilitating comparisons with earlier studies, is to evaluate the consequence on the SDCF of simultaneously omitting hysteresis and chemical composition. Specifically, particle composition assumes full neutralization (i.e., $X = 1$), and hysteresis is omitted using DRH = CRH$_0$ = 35%. This approach, used in several previous studies [Koch et al., 1999; Schulz et al., 2006], overestimates the SDCF$_{fky}$ by +8% relative to the base case (Table 3). Moreover, simplifying the aerosol optical properties by using $\overline{\beta}_{aq} = \overline{\beta}_{sd}$ (i.e., $g_{aq} = g_{sd}$) increases the overestimate to +26%. In comparison, using $\overline{\beta}_{aq} = \overline{\beta}_{sd}$ but otherwise retaining the base case overestimates SDCF$_{fky}$ by +15% (Table 3). These biases explain in part why the NSDCF of our base case is less than the mean of the intercomparison of Schulz et al. [2006] (Table 4).

6. Conclusions

[39] The impact of sulfate particles on the radiative forcing of climate depends strongly on their water content. The hysteresis effect of sulfate phase transitions complicates the treatment of water content in models. We explored this issue using a column model of sulfate direct climate forcing to investigate the relative influences of the differing key parameters of solid compared to aqueous particles, such as extinction coefficients, backscattered fractions, and growth factors. We then used a global 3-D chemical transport model for the sulfate-ammonium system to examine systematically the dependence of sulfate direct climate forcing on different approaches for treating the hysteresis effect.

[40] In our base case of the CTM simulation with full consideration of the hysteresis loop and natural and anthropogenic emissions, we find that solid particles contribute 34% of the sulfate burden, 20% of the aerosol optical thickness, and 34% of the full-sky radiative effect, as global and annual averages, with the balance in all cases from aqueous particles. The direct radiative effect of full-sky compared to clear-sky conditions is 55% for solid particles and 35% for aqueous particles. The different ratios reflect the relative correlations of solid and aqueous particles with clouds. For the anthropogenic component, solid particles contribute 41% of the sulfate burden, 26% of the optical thickness, and 37% of the full-sky sulfate direct climate forcing, as global annual averages.

[41] A sensitivity study that omits the hysteresis effect by using all aqueous particles (i.e., CRH = DRH = 0) overestimates the full-sky climate forcing by +8% compared to the base case. Omission of the hysteresis effect by assuming that solid particles readily form (i.e., CRH = DRH_0) underestimates the forcing by −8%. Omitting the hysteresis by assuming DRH = CRH_0 overestimates forcing by +5%. The estimates of global annual average forcing therefore differ by up to 16%, depending on the approach for treating (or omitting) hysteresis. Regional differences, however, can be larger than 20%, mainly near SO_2 source regions where the regional forcing is the largest. The global annual difference from the base case can increase to 26% in the case of a model that omits the differences between the backscattered fractions of aqueous compared to solid particles, while simultaneously assuming $X = 1$ and CRH = DRH_0 (i.e., precisely as done in some CTMs) (see discussion by *Kiehl et al.* [2000]). Given these uncertainties of model predictions on the treatment of phase transitions, we recommend that the normalized growth factor of aerosol optical thickness, defined as the ratio of sulfate optical thickness with versus without considering aerosol hygroscopicity, should be reported in future studies as a normalization for analyzing and explaining discrepancies among forcing estimates of different CTMs.

[42] Our current study was limited to the sulfate-ammonium system and analyzed only the impact of aerosol phase transitions on the sulfate direct climate forcing. In ambient air, phase transitions of sulfate particles are more complicated, including effects by organic molecules and nitrate content that tend to decrease CRH and DRH and insoluble components such as mineral dust that tend to increase CRH [*Martin et al.*, 2003, 2004]. *Wang et al.* [2008] investigated how shifts from −30% to +45% in CRH affected the modeled burden of solids. *Martin et al.* [2004] found that evaporation of ammonium nitrate driven by the crystallization of sulfate-nitrate-ammonium particles can change forcing by 20%.

[43] Future emissions of SO_2 are anticipated to decrease (at least over North America and Europe) as a result of clean air regulation. Ammonia emissions and consequently the atmospheric concentrations of NH_3 are expected to rise more quickly than those of acidic species. The implication of these trends is greater neutralization of atmospheric particles, a condition favoring crystallization and thus suggesting a growing importance of particle phase transitions in a quantitative understanding of atmospheric chemistry and climate.

References

Adams, P., J. H. Seinfeld, and D. M. Koch (1999), Global concentrations of tropospheric sulfate, nitrate, and ammonium aerosol simulated in a general circulation model, *J. Geophys. Res.*, 104, 13,791–13,823, doi:10.1029/1999JD900083.

Adams, P. J., J. H. Seinfeld, D. Koch, L. Mickely, and D. Jacob (2001), General circulation model assessment of direct radiative forcing by the sulfate-nitrate-ammonium-water inorganic aerosol system, *J. Geophys. Res.*, 106, 1097–1111, doi:10.1029/2000JD900512.

Anderson, T. L., et al. (2005), An "A-Train" strategy for quantifying direct climate forcing by anthropogenic aerosols, *Bull. Am. Meteorol. Soc.*, 86, 1795–1809, doi:10.1175/BAMS-86-12-1795.

Boer, G. J., I. N. Sokolik, and S. T. Martin (2007a), Infrared optical constants of aqueous sulfate-nitrate-ammonium multi-component tropospheric aerosols from attenuated total reflectance measurements: Part I. Results and analysis of spectral absorbing features, *J. Quant. Spectrosc. Radiat. Transfer*, 108, 17–38, doi:10.1016/j.qsrt.2007.02.017.

Boer, G. J., I. N. Sokolik, and S. T. Martin (2007b), Infrared optical constants of aqueous sulfate-nitrate-ammonium multi-component tropospheric aerosols from attenuated total reflectance measurements: Part II. An examination of mixing rules, *J. Quant. Spectrosc. Radiat. Transfer*, 108, 39–53, doi:10.1016/j.qsrt.2007.02.018.

Boucher, O., and T. L. Anderson (1995), GCM assessment of the sensitivity of direct climate forcing by anthropogenic sulfate aerosols to aerosol size and chemistry, *J. Geophys. Res.*, 100, 26,117–26,134, doi:10.1029/95JD02531.

Charlson, R. J., S. E. Schwartz, J. M. Hales, R. D. Cess, J. A. Coakley, J. E. Hansen, and D. J. Hoffman (1992), Climate forcing by anthropogenetic aerosols, *Science*, 255, 423–430, doi:10.1126/science.255.5043.423.

Chuang, C. C., J. E. Penner, K. E. Taylor, A. S. Grossman, and J. J. Walton (1997), An assessment of the radiative effects of anthropogenic sulfate, *J. Geophys. Res.*, 102, 3761–3778, doi:10.1029/96JD03087.

Colberg, C. A., B. P. Luo, H. Wernli, T. Koop, and T. Peter (2003), A novel model to predict the physical state of atmospheric $H_2SO_4/NH_3/H_2O$ aerosol particles, *Atmos. Chem. Phys.*, 3, 909–924.

Crutzen, P. J. (2006), Albedo enhancement by stratospheric sulfur injections: A contribution to resolve a policy dilemma?, *Clim. Change*, 77, 211–219, doi:10.1007/s10584-006-9101-y.

Dentener, F., et al. (2006), Emissions of primary aerosol and precursor gases in the years 2000 and 1750 prescribed data-sets for AeroCom, *Atmos. Chem. Phys.*, 6, 4321–4344.

Fu, Q., and K. N. Liou (1993), Parameterization of the radiative properties of cirrus clouds, *J. Atmos. Sci.*, 50, 2008–2025, doi:10.1175/1520-0469(1993)050<2008:POTRPO>2.0.CO;2.

Ghan, S., N. Laulaninen, R. Easter, R. Wagener, S. Nemesure, E. Chapman, Y. Zhang, and R. Leung (2001), Evaluation of aerosol direct forcing in MIRAGE, *J. Geophys. Res.*, 106, 5295–5316, doi:10.1029/2000JD900502.

Hansen, J. E., and L. D. Travis (1974), Light scattering in planetary atmospheres, *Space Sci. Rev.*, 16, 527–610, doi:10.1007/BF00168069.

Hansen, J., et al. (2005), Earth's energy imbalance: confirmation and implications, *Science*, 308, 1431–1435, doi:10.1126/science.1110252.

Haywood, J., D. L. Roberts, A. Slingo, J. M. Edwards, and K. P. Shine (1997), General circulation model calculations of the direct radiative forcing by anthropogenic sulfate and fossil-fuel soot aerosol, *J. Clim.*, 10, 1562–1577, doi:10.1175/1520-0442(1997)010<1562:GCMCOT>2.0.CO;2.

Hess, M., P. Koepke, and I. Schult (1998), Optical properties of aerosols and clouds: The software package OPAC, *Bull. Am. Meteorol. Soc.*, 79, 831–844, doi:10.1175/1520-0477(1998)079<0831:OPOAAC>2.0.CO;2.

Intergovernmental Panel on Climate Change (2001), *Climate Change 2001: The Scientific Basis—Contribution of Working Group I to the Third Assessment Report of the Intergovernmental Panel on Climate Change*, edited by J. T. Houghton et al., Cambridge Univ. Press, New York.

Intergovernmental Panel on Climate Change (2007), *Climate Change 2007: The Physical Science Basis—Contribution of Working Group I to the Fourth Assessment. Report of the Intergovernmental Panel on Climate Change*, edited by S. Solomon et al., Cambridge Univ. Press, New York.

Jacob, D. J., et al. (2005), *Radiative Forcing of Climate Change: Expanding the Concept and Addressing Uncertainties*, Natl. Res. Counc., Washington, D. C.

Kiehl, J. T., and B. P. Briegleb (1993), The radiative roles of sulfate aerosols and greenhouse gases in climate forcing, *Science*, 260, 311–314, doi:10.1126/science.260.5106.311.

Kiehl, J. T., T. L. Schneider, P. J. Rasch, M. C. Barth, and J. Wong (2000), Radiative forcing due to sulfate aerosols from simulations with the National Center for Atmospheric Research Community Climate Model, Version 3, *J. Geophys. Res.*, 105, 1441–1457, doi:10.1029/1999JD900495.

Kinne, S., et al. (2006), An AeroCom initial assessment—Optical properties in aerosol component modules of global models, *Atmos. Chem. Phys.*, 6, 1815–1834.

Koch, D. (2001), Transport and direct radiative forcing of carbonaceous and sulfate aerosols in the GISS GCM, *J. Geophys. Res.*, 106, 20,311–20,332, doi:10.1029/2001JD900038.

Koch, D., D. Jacob, I. Tegen, D. Rind, and M. Chin (1999), Tropospheric sulfur simulation and sulfate direct radiative forcing in the Goddard

Institute for Space Studies general circulation model, *J. Geophys. Res.*, *104*, 23,799–23,822, doi:10.1029/1999JD900248.

Koelemeijer, R. B. A., J. F. de Haan, and P. Stammes (2003), A database of spectral surface reflectivity in the range 335–772 nm derived from 5.5 years of GOME observations, *J. Geophys. Res.*, *108*(D2), 4070, doi:10.1029/2002JD002429.

Liu, H., et al. (2006), Radiative effect of clouds on tropospheric chemistry in a global three-dimensional chemical transport model, *J. Geophys. Res.*, *111*, D20303, doi:10.1029/2005JD006403.

Martin, S. T. (2000), Phase transitions of aqueous atmospheric particles, *Chem. Rev.*, *100*, 3403–3453, doi:10.1021/cr990034t.

Martin, S. T., J. C. Schlenker, A. Malinowski, H. Hung, and Y. Rudich (2003), Crystallization of atmospheric sulfate-nitrate-ammonium particles, *Geophys. Res. Lett.*, *30*(21), 2102, doi:10.1029/2003GL017930.

Martin, S. T., H. M. Hung, R. J. Park, D. J. Jacob, R. J. D. Spurr, K. V. Chance, and M. Chin (2004), Effects of the physical state of tropospheric ammonium-sulfate-nitrate particles on global aerosol direct radiative forcing, *Atmos. Chem. Phys.*, *4*, 183–214.

Nemesure, S., R. Wagener, and S. E. Schwartz (1995), Direct shortwave forcing of climate by the anthropogenic sulfate aerosol: Sensitivity to particle size, composition, and relative humidity, *J. Geophys. Res.*, *100*, 26,105–26,116, doi:10.1029/95JD02897.

Onasch, T. B., R. L. Siefert, S. D. Brooks, A. J. Prenni, B. Murray, M. A. Wilson, and M. A. Tolbert (1999), Infrared spectroscopic study of the deliquescence and efflorescence of ammonium sulfate aerosol as a function of temperature, *J. Geophys. Res.*, *104*, 21,317–21,326, doi:10.1029/1999JD900384.

Park, R. J., D. J. Jacob, B. D. Field, R. M. Yantosca, and M. Chin (2004), Natural and transboundary pollution influences on sulfate-nitrate-ammonium aerosols in the United States: Implications for policy, *J. Geophys. Res.*, *109*, D15204, doi:10.1029/2003JD004473.

Penner, J. E., C. C. Chuang, and K. Grant (1998), Climate forcing by carbonaceous and sulfate aerosols, *Clim. Dyn.*, *14*, 839–851, doi:10.1007/s003820050259.

Reddy, M. S., O. Boucher, N. Bellouin, M. Schulz, Y. Ballkanski, J.-L. Dufresne, and M. Pham (2005), Estimates of global multicomponent aerosol optical depth and direct radiative perturbation in the Laboratoire de Meteorologie Dynamique general circulation model, *J. Geophys. Res.*, *110*, D10S16, doi:10.1029/2004JD004757.

Schlenker, J. C., and S. T. Martin (2005), Crystallization pathways of sulfate-nitrate-ammonium aerosol particles, *J. Phys. Chem. A*, *109*, 9980–9985, doi:10.1021/jp052973x.

Schlenker, J. C., A. Malinowski, S. T. Martin, H. M. Hung, and Y. Rudich (2004), Crystals formed at 293 K by aqueous sulfate-nitrate-ammonium-proton aerosol particles, *J. Phys. Chem. A*, *108*, 9375–9383, doi:10.1021/jp047836z.

Schulz, M., et al. (2006), Radiative forcing by aerosols as derived from the AeroCom present-day and pre-industrial simulations, *Atmos. Chem. Phys.*, *6*, 5225–5246.

Tang, I. N. (1996), Chemical and size effects of hygroscopic aerosols on light scattering coefficient, *J. Geophys. Res.*, *101*, 19,245–19,250, doi:10.1029/96JD03003.

Tang, I. N., and H. R. Munkelwitz (1994), Water activities, densities, and refractive indices of aqueous sulfates and sodium nitrate droplets of atmosphere importance, *J. Geophys. Res.*, *99*, 18,801–18,808, doi:10.1029/94JD01345.

Wang, J., and S. T. Martin (2007), Satellite characterization of urban aerosols: Importance of including hygroscopicity and mixing state in retrieval algorithms, *J. Geophys. Res.*, *112*, D17203, doi:10.1029/2006JD008078.

Wang, J., S. A. Christopher, F. Brechtel, J. Kim, B. Schmid, J. Redemann, P. B. Russell, P. Quinn, and B. N. Holben (2003), Geostationary satellite retrievals of aerosol optical thickness during ACE-Asia, *J. Geophys. Res.*, *108*(D23), 8657, doi:10.1029/2003JD003580.

Wang, J., U. Nair, and S. A. Christopher (2004), GOES-8 aerosol optical thickness assimilation in a mesoscale model: Online integration of aerosol radiative effects, *J. Geophys. Res.*, *109*, D23203, doi:10.1029/2004JD004827.

Wang, J., A. A. Hoffmann, R. J. Park, D. J. Jacob, and S. T. Martin (2008), Global distribution of solid and aqueous sulfate aerosols: Effect of the hysteresis of particle phase transitions, *J. Geophys. Res.*, *113*, D11206, doi:10.1029/2007JD009367.

Wiscombe, W. J., and G. W. Grams (1976), The backscattered fraction in two-stream approximations, *J. Atmos. Sci.*, *33*, 2440–2451, doi:10.1175/1520-0469(1976)033<2440:TBFITS>2.0.CO;2.

Yu, H., et al. (2006), A review of measurement–based assessment of aerosol direct radiative effect and forcing, *Atmos. Chem. Phys.*, *6*, 613–666.

————————————

D. J. Jacob and S. T. Martin, School of Engineering and Applied Sciences, Harvard University, Cambridge, MA 02138, USA. (scot_martin@harvard.edu)

J. Wang, Department of Geosciences, University of Nebraska–Lincoln, Lincoln, NE 68588, USA. (jwang7@unl.edu)